HHS Public Access

Author manuscript

Angew Chem Int Ed Engl. Author manuscript; available in PMC 2024 February 01.

Published in final edited form as:

Angew Chem Int Ed Engl. 2023 February 01; 62(6): e202214920. doi:10.1002/anie.202214920.

A Fluorogenic Inhibitor of the Mitochondrial Calcium Uniporter

Zhouyang Huang[a], **Samantha N. MacMillan**[a], **Justin J. Wilson**[a]

[a]Department of Chemistry and Chemical Biology, Cornell University, Ithaca, New York 14853, United States

Abstract

Inhibitors of the mitochondrial calcium uniporter (MCU) are valuable tools for studying the role of mitochondrial Ca^{2+} in various pathophysiological conditions. In this study, a new fluorogenic MCU inhibitor, **RuOCou**, is presented. This compound is an analogue of the known MCU inhibitor Ru265 that contains fluorescent axial coumarin carboxylate ligands. Upon aquation of **RuOCou** and release of the axial coumarin ligands, a simultaneous increase in its MCU-inhibitory activity and fluorescence intensity is observed. The fluorescence response of this compound enabled its aquation to be monitored in both HeLa cell lysates and live HeLa cells. This fluorogenic prodrug represents a potential theranostic MCU inhibitor that can be leveraged for the treatment of human diseases related to MCU activity.

Graphical Abstract

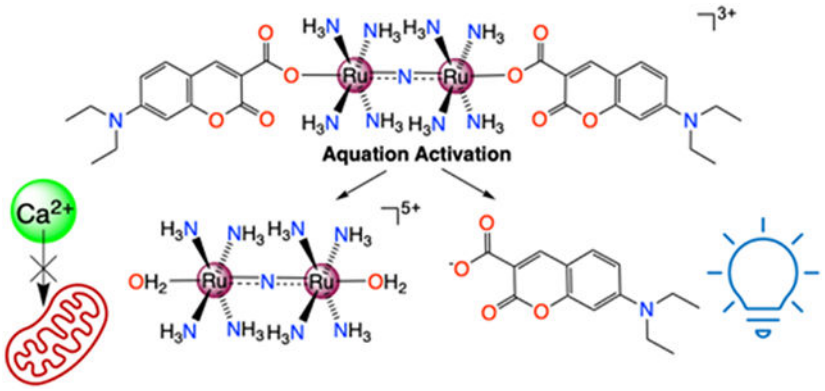

RuOCou is a novel fluorogenic inhibitor of mitochondria calcium uniporter (MCU). Its aquation-activated increase in MCU-inhibitory activity can be visualized directly by a concomitant enhancement in fluorescence intensity.

Keywords

Bioinorganic chemistry; Fluorescent probes; Mitochondrial calcium uniporter; Prodrugs; Ruthenium

jjw275@cornell.edu, Institute and/or researcher Twitter usernames: @JWilsonLab.

The mitochondrial calcium uniporter (MCU) is a highly selective ion channel that is responsible for shuttling Ca^{2+} into mitochondria.[1-3] Dysregulation of the MCU can trigger an overload of mitochondrial Ca^{2+} ($m$$Ca^{2+}$) levels, leading to deleterious conditions including neurodegeneration,[4-7] ischemia-reperfusion injury,[8,9] and cancer.[10-12] Therefore, molecules that can inhibit the MCU are valuable for understanding the role of $m$$Ca^{2+}$ dynamics in humans.[13,14] Among small-molecule MCU inhibitors, Ru coordination complexes are the most prominent, as evidenced by the widespread use of the established compounds ruthenium red and Ru360 for this application[15-19] and the significant ongoing efforts to develop new analogues. For instance, our group has identified a dinuclear nitrido-bridged Ru complex $[Cl(NH_3)_4Ru(\mu\text{-}N)Ru(NH_3)_4Cl]^{3+}$, named Ru265, to be a potent MCU inhibitor that protects against in vitro hypoxia-reoxygenation and an in vivo model of ischemic stroke.[20,21] The current mechanistic understanding is that Ru265 first aquates to the diaqua-capped $[(OH_2)(NH_3)_4Ru(\mu\text{-}N)Ru(NH_3)_4(OH_2)]^{5+}$ (Ru265′) with a half-life of several minutes under physiological conditions[22,23] (Scheme 1), and Ru265′ inhibits $m$$Ca^{2+}$ by binding to a highly conserved and exposed peptide sequence, known as the DIME region, of the MCU pore.[24] The $(NH_3)_4Ru(\mu\text{-}N)Ru(NH_3)_4$ core is critical for the MCU-inhibitory activity of Ru265, but the axial chloride ligands can be altered to optimize the biological properties of this compound. For example, we recently reported that analogues of Ru265 bearing axial carboxylates instead of chlorides undergo aquation on the timescale of hours under physiological conditions, releasing the potent MCU inhibitor Ru265′.[25] Thus, modification of the axial ligand of Ru265 can afford promising MCU inhibitor prodrugs with tunable properties.

Although Ru265 and its analogues possess useful biological properties, they are not amenable to non-invasive imaging due to their lack of appropriate spectroscopic or nuclear properties. To fill this gap, we sought to impart fluorescent properties upon Ru265 by functionalizing the axial ligands. In particular, the introduction of well-established coumarin-based fluorophores[26,27] to the axial position of this complex would be a promising approach, because coumarin-containing metal complexes have been extensively investigated for their photophysical properties, cellular imaging applications, and antiproliferative effects.[28-31] Specifically, 7-diethylaminocoumarin-3-carboxylate ($OCou^-$) was chosen as the axial ligand because its intrinsic mitochondria-targeting properties[32-35] could be potentially beneficial for delivering the Ru complex to this organelle for enhanced efficacy of $m$$Ca^{2+}$ uptake inhibitory activity. Herein, we present the synthesis, physical characterization, and biological properties of a coumarin-capped analogue of Ru265, named **RuOCou** (Scheme 1).

RuOCou was prepared using a method that was previously reported for the synthesis of carboxylate-capped Ru265 derivatives.[25] In short, Ru265 was allowed to react with 5 equiv of AgOTf in water to remove both the outer- and inner-sphere chlorides as insoluble AgCl and produce the diaqua-capped synthon Ru265'. Treatment of Ru265' with $OCou^-$ afforded **RuOCou**, which was fully characterized using NMR and IR spectroscopy (Figures S2-S5) as well as X-ray crystallography (Figure 1 and Tables S1 and S2). The crystal structure of the complex reveals the expected geometry, comprising an almost linear Ru(μ-N)Ru core (172.9(1)°) with eight equatorial NH_3 ligands and two axial $OCou^-$ ligands.[36] Overall,

the Ru–N and Ru–O interatomic distances agree well with previously reported carboxylate-capped Ru265 derivatives.[25]

Next, the aquation kinetics of **RuOCou** in pH 7.4 MOPS buffer at 37 °C were determined by UV-vis spectroscopy (Figure S6). The aquation half-life of **RuOCou** is 2.1 h (Table 1), which is within the range reported for other carboxylate derivatives of Ru265 (3.3–9.9 h).[25] We also monitored this process under the same conditions by fluorescence spectroscopy. Over time, an increase in fluorescence intensity is observed (Figure 2). The rate of the emission increase ($t_{1/2}$ = 2.2 h) is almost identical to the spectroscopic changes measured by UV-vis spectroscopy, indicating that the enhancement of fluorescence is a consequence of aquation. In this case, a likely explanation for this emission increase is that the fluorescence of the coumarin ligand is quenched when coordinated to the Ru centers. Leveraging the sensitivity of fluorescence spectroscopy, we also measured the aquation kinetics of **RuOCou** in HeLa cell lysates, revealing a similar rate of activation ($t_{1/2}$ = 3.5 h) within these biological conditions (Figure S7). In consideration of a possible cellular uptake of this complex through endocytosis, we also evaluated the aquation kinetics under the more acidic conditions found in the lysosomes. Notably, the aquation half-life at pH 5 ($t_{1/2}$ = 2.6 h) as measured by UV-vis spectroscopy (Figure S8) is not substantially different than that at pH 7.4, indicating that dissociation of the complex is not accelerated under acidic conditions.

To further understand the mechanism of fluorescence quenching of $OCou^-$ upon coordination to Ru, we performed density functional theory (DFT) and (time-dependent density functional theory) TD-DFT calculations. The frontier molecular orbitals (FMOs) of the DFT-optimized structures of **RuOCou** and the free ligand $OCou^-$ are shown in Figure 3. The highest occupied molecular orbital (HOMO) of $OCou^-$ and HOMO–1 (H-1) and HOMO of **RuOCou** are coumarin-based **π** orbitals, as are the lowest unoccupied molecular orbital (LUMO) of $OCou^-$ and LUMO+2 (L+2) and L+3 of the **RuOCou**. In comparing relative energies, these coumarin-based orbitals are lower in **RuOCou**, indicating that they are stabilized upon coordination to Ru. Within **RuOCou**, the LUMO and L+1 are delocalized Ru–N–Ru **π*** orbitals, which reside energetically between the coumarin-based **π** orbitals. Upon photoexcitation of **RuOCou** to the emissive coumarin **π-π*** excited state, the LUMO and L+1 provide an energetically viable pathway for photoinduced electron transfer (PET) that outcompetes the radiative decay process.[27,37] TD-DFT calculations, which determine the energies of electronic states rather than orbitals, also support this hypothesis (Figure S9). In the case of $OCou^-$, the lowest energy singlet excited state is coumarin-based with a high oscillator strength. For **RuOCou**, however, there are 12 excited states, all with small oscillator strengths, that are lower in energy than this coumarin-based **π-π*** excited state. Consistent with the simple orbital energy arguments above, these low-energy excited states, most of which are metal-based, are likely responsible for quenching the photoluminescent coumarin-based excited state. The careful positioning of metal-based orbitals or excited states to quench fluorophores via PET is a common strategy for designing fluorescent chemosensors based on dyes like coumarins.[26,27]

With a deeper understanding of its photophysical properties, we next evaluated the biological properties of **RuOCou**. Freshly prepared solutions of **RuOCou** inhibit $m\mathrm{Ca}^{2+}$ uptake in permeabilized HEK293T cells with nanomolar potency (Table 1), but at levels

that are still 8-fold lower than those of Ru265. Allowing solutions of **RuOCou** to age and undergo aquation, however, leads to an increase in MCU-inhibitory activity, which reaches the same level as Ru265 after 20 h (Figure 4). Thus, like other carboxylate-capped analogues of Ru265, **RuOCou** can potentially be used as an aquation-activated prodrug.[25] Encouraged by these results in permeabilized cells, we proceeded to study **RuOCou** in intact cells. Cellular uptake studies reveal that **RuOCou** accumulates at 10-fold higher concentrations in HEK293T cells compared to Ru265 (Table 1). This improved uptake may be a consequence of the greater lipophilicity of the axial coumarin ligands present within **RuOCou**. Moreover, like Ru265, **RuOCou** can inhibit mCa^{2+} uptake in intact HeLa cells without compromising the mitochondrial membrane potential, as demonstrated by Rhod2AM (Figure S13) and JC-1 (Figure S14) assays, respectively. Lastly, **RuOCou** exhibits only minimal cytotoxicity with an IC_{50} of 56 μM in HEK293T cells after 48 h incubation (Table 1). The complex is moderately more toxic in HeLa cells with an IC_{50} of 33 μM under the same condition (Figure S10).

Leveraging the photophysical properties of **RuOCou,** we examined its intracellular accumulation by using confocal fluorescence microscopy. Prior to imaging, HeLa cells were incubated for 24 h with either 40 μM OCou$^-$ or 20 μM **RuOCou.** The average fluorescent intensity within the **RuOCou**-treated cells was found to be 2-fold higher than the OCou$^-$-treated cells (Figure S15). This result suggests that coordination of OCou$^-$ to Ru enhances its cellular uptake. Moreover, these data also imply that the rate of cellular uptake of **RuOCou** is faster than its aquation. If **RuOCou** were to aquate before being internalized, the improved uptake of the coumarin ligands would not be observed. To assess the intracellular localization of **RuOCou**, HeLa cells were co-treated with **RuOCou** and different organelle stains prior to imaging. The complex does not appreciably accumulate in the nucleus (Figure S16). In contrast, as shown in Figure 5, the signals within the blue (**RuOCou**) and red (MitoTracker Red) channels showed a strong colocalization, as reflected by a Pearson's correlation coefficient of 0.75 ± 0.04, indicating that **RuOCou** or the OCou$^-$ delivered by the complex accumulates in the mitochondria. This result is consistent with the previously reported abilities of both the coumarin ligand[32-35] and Ru265[20] to enter this organelle. It is worth noting that, an appreciable amount of lysosomal accumulation was also observed for **RuOCou**, as reflected by a Pearson's correlation coefficient of 0.68 ± 0.06 between the complex and LysoTracker Red DND-99 (Figure S17).

Having confirmed that **RuOCou** can be imaged by fluorescence microscopy, we finally sought to demonstrate its aquation-triggered fluorescence turn-on in intact living cells. HeLa cells were treated with **RuOCou** for 30 min, thoroughly washed, and subsequently imaged for another 40 min. We employed a high concentration of **RuOCou** (75 μM) in this experiment to maximize the fluorescent signals. Even though this concentration is higher than the IC_{50} value, no cytotoxic effects were observed over this short incubation period. As shown in Figure 6, a modest yet statistically significant enhancement (2-fold) in fluorescent intensity was observed during this time-period. The small magnitude of the turn-on response, compared to the studies in buffer and cell lysates, is likely due to the 30 min preincubation period required for this experiment, which is long enough for partial aquation of **RuOCou** to occur before imaging. Nevertheless, these results still represent the

proof of concept for tracking fluorogenic MCU inhibitors in living cells and monitoring their activation processes in real time.

In summary, **RuOCou** is a novel fluorogenic MCU inhibitor. Its aquation-activated increase in MCU-inhibitory activity can be visualized directly by a concomitant enhancement in fluorescence intensity. This study serves as the first proof of principle for the real-time visualization of MCU-inhibition in living cells, which is an important step towards establishing a deeper understanding of the mitochondrial calcium dynamics. Ongoing efforts are directed at developing new analogues with longer aquation half-lives which would allow easier visualization of the turn-on effect and better control of the biological properties of this compound class. We are also investigating the use of near-infrared-emitting fluorophores that would provide better biological compatibility and a deeper penetration range. Finally, we are seeking alternative stimuli for triggering the fluorogenic responses, which would enable a greater spatiotemporal control of the activation.

Supplementary Material

Refer to Web version on PubMed Central for supplementary material.

Acknowledgements

This research was supported by Cornell University and the NSF under award number CHE-1750295. This work made use of the Cornell University NMR facility, which is supported by the NSF under award number CHE-1531632. Additional resources included the use of the Cornell University Biotechnology Resource Center (BRC), which is supported by the NIH (NIH S10RR025502). Dr. Johanna Dela Cruz from Cornell BRC is thanked for assistance in confocal fluorescent microscopy.

References

[1]. Kirichok Y, Krapivinsky G, Clapham DE, Nature 2004, 427, 360–364. [PubMed: 14737170]

[2]. Kamer KJ, Mootha VK, Nat. Rev. Mol. Cell Biol 2015, 16, 545–553. [PubMed: 26285678]

[3]. Nemani N, Shanmughapriya S, Madesh M, Cell Calcium 2018, 74, 86–93. [PubMed: 29980025]

[4]. Devine MJ, Kittler JT, Nat. Rev. Neurosci 2018, 19, 63–80.

[5]. Lee K-S, Huh S, Lee S, Wu Z, Kim A-K, Kang H-Y, Lu B, Proc. Natl. Acad. Sci. U. S. A 2018, 115, E8844–E8853. [PubMed: 30185553]

[6]. Pchitskaya E, Popugaeva E, Bezprozvanny I, Cell Calcium 2018, 70, 87–94. [PubMed: 28728834]

[7]. Nam E, Han J, Suh J-M, Yi Y, Lim MH, Curr. Opin. Chem. Biol 2018, 43, 8–14. [PubMed: 29100100]

[8]. Shintani-Ishida K, Inui M, Yoshida K, J. Mol. Cell. Cardiol 2012, 53, 233–239. [PubMed: 22659291]

[9]. Lesnefsky EJ, Chen Q, Tandler B, Hoppel CL, Annu. Rev. Pharmacol. Toxicol 2017, 57, 535–565. [PubMed: 27860548]

[10]. Bong AHL, Monteith GR, Biochim. Biophys. Acta - Mol. Cell Res 2018, 1865, 1786–1794. [PubMed: 29842892]

[11]. Vultur A, Gibhardt CS, Stanisz H, Bogeski I, Pflugers Arch. Eur. J. Physiol 2018, 470, 1149–1163. [PubMed: 29926229]

[12]. Delierneux C, Kouba S, Shanmughapriya S, Potier-Cartereau M, Trebak M, Hempel N, Cells 2020, 9, 432. [PubMed: 32059571]

[13]. De Mario A, Tosatto A, Hill JM, Kriston-Vizi J, Ketteler R, Vecellio Reane D, Cortopassi G, Szabadkai G, Rizzuto R, Mammucari C, Cell Rep. 2021, 35, 109275. [PubMed: 34161774]

[14]. Woods JJ, Wilson JJ, Curr. Opin. Chem. Biol 2020, 55, 9–18. [PubMed: 31869674]

[15]. Matlib MA, Zhou Z, Knight S, Ahmed S, Choi KM, Krause-Bauer J, Phillips R, Altschuld R, Katsube Y, Sperelakis N, Bers DM, J. Biol. Chem 1998, 273, 10223–10231. [PubMed: 9553073]

[16]. Emerson J, Clarke MJ, Ying W-L, Sanadi DR, J. Am. Chem. Soc 1993, 115, 11799–11805.

[17]. Ying W-L, Emerson J, Clarke MJ, Sanadi DR, Biochemistry 1991, 30, 4949–4952. [PubMed: 2036363]

[18]. Nathan SR, Pino NW, Arduino DM, Perocchi F, MacMillan SN, Wilson JJ, Inorg. Chem 2017, 56, 3123–3126. [PubMed: 28244741]

[19]. Cervinka J, Gobbo A, Biancalana L, Markova L, Novohradsky V, Guelfi M, Zacchini S, Kasparkova J, Brabec V, Marchetti F, J. Med. Chem 2022, 65, 10567–10587. [PubMed: 35913426]

[20]. Woods JJ, Nemani N, Shanmughapriya S, Kumar A, Zhang M, Nathan SR, Thomas M, Carvalho E, Ramachandran K, Srikantan S, Stathopulos PB, Wilson JJ, Madesh M, ACS Cent. Sci 2019, 5, 153–166. [PubMed: 30693334]

[21]. Novorolsky RJ, Nichols M, Kim JS, Pavlov EV, J Woods J, Wilson JJ, Robertson GS, Cereb J. Blood Flow Metab. 2020, 40, 1172–1181.

[22]. Woods JJ, Lovett J, Lai B, Harris HH, Wilson JJ, Angew. Chem. Int. Ed 2020, 59, 6482–6491.

[23]. Woods JJ, Spivey JA, Wilson JJ, Eur. J. Inorg. Chem 2022, 2022, e202100995.

[24]. Woods JJ, Rodriguez MX, Tsai C-W, Tsai M-F, Wilson JJ, Chem. Commun 2021, 57, 6161–6164.

[25]. Bigham NP, Huang Z, Spivey J, Woods JJ, MacMillan SN, Wilson JJ, Inorg. Chem 2022, 61, 17299–17312. [PubMed: 36260092]

[26]. Cao D, Liu Z, Verwilst P, Koo S, Jangjili P, Kim JS, Lin W, Chem. Rev 2019, 119, 10403–10519. [PubMed: 31314507]

[27]. Sun X, Liu T, Sun J, Wang X, RSC Adv. 2020, 10, 10826–10847. [PubMed: 35492912]

[28]. Grazul M, Budzisz E, Coord. Chem. Rev 2009, 253, 2588–2598.

[29]. Balcıoğlu S, Olgun Karataş M, Ateş B, Alıcı B, Özdemir İ, Bioorg. Med. Chem. Lett 2020, 30, 126805. [PubMed: 31753700]

[30]. Balewski Ł, Szulta S, Jalińska A, Kornicka A, Front. Chem 2021, 9, 781779. [PubMed: 34926402]

[31]. Patil SA, Kandathil V, Sobha A, Somappa SB, Feldman MR, Bugarin A, Patil SA, Molecules 2022, 27, 5220. [PubMed: 36014460]

[32]. Zhang X, Ba Q, Gu Z, Guo D, Zhou Y, Xu Y, Wang H, Ye D, Liu H, Chem. Eur. J 2015, 21, 17415–17421. [PubMed: 26458147]

[33]. Cai G, Yu W, Song D, Zhang W, Guo J, Zhu J, Ren Y, Kong L, Eur. J. Med. Chem 2019, 174, 236–251. [PubMed: 31048139]

[34]. Yang K, Li Y, Tang Q, Zheng L, He D, Eur. J. Med. Chem 2019, 170, 45–54. [PubMed: 30878831]

[35]. Tu Y, Li H-M, Wang M-M, Su Y, Liu H-K, Su Z, Eur. J. Inorg. Chem 2022, 2022, e202200184.

[36]. Deposition number: 2212060 contains the supplementary crystallographic data for this paper. These data are provided free of charge bythe joint Cambridge Crystallographic Data Centre and Fachin-formationszentrum Karlsruhe Access Structures service.

[37]. Fu Y, Finney NS, RSC Adv. 2018, 8, 29051–29061. [PubMed: 35547972]

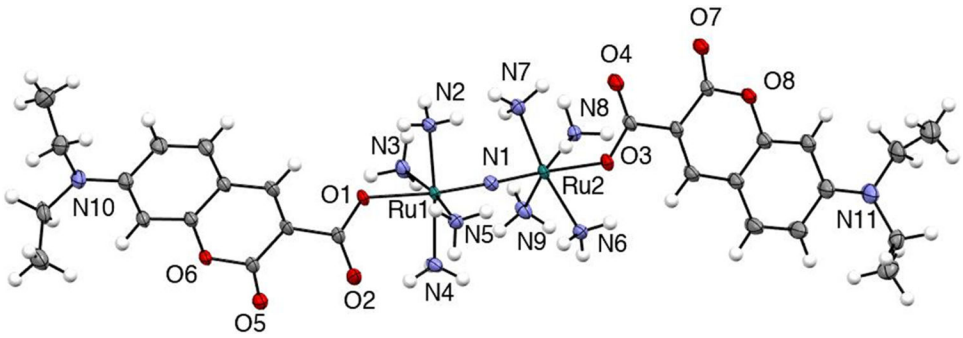

Figure 1.

Crystal structure of **RuOCou**. Thermal ellipsoids are shown at the 50% probability level. Solvents and counterions are omitted for clarity.

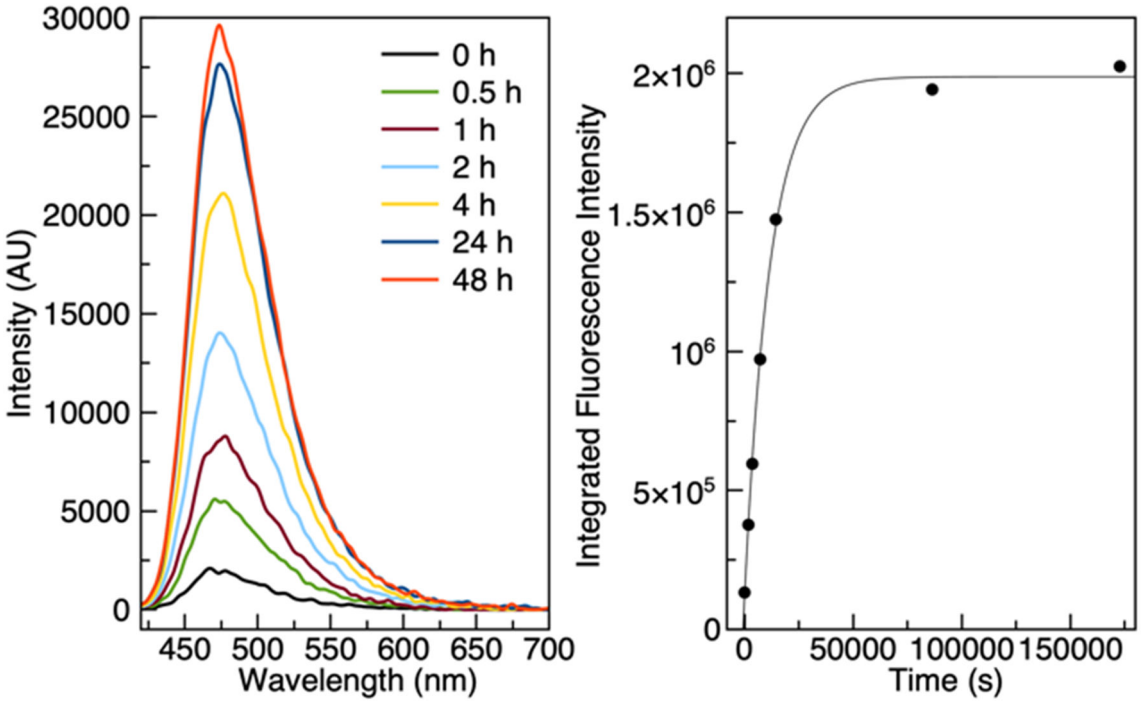

Figure 2.

Left: evolution of the emission spectrum of **RuOCou** (1 μM) in pH 7.4 MOPS-buffered (100 μM) aqueous solution over a 48 h period at 37 °C (excitation wavelength: 402 nm). Right: plot of integrated fluorescence intensity versus time with the best exponential fit.

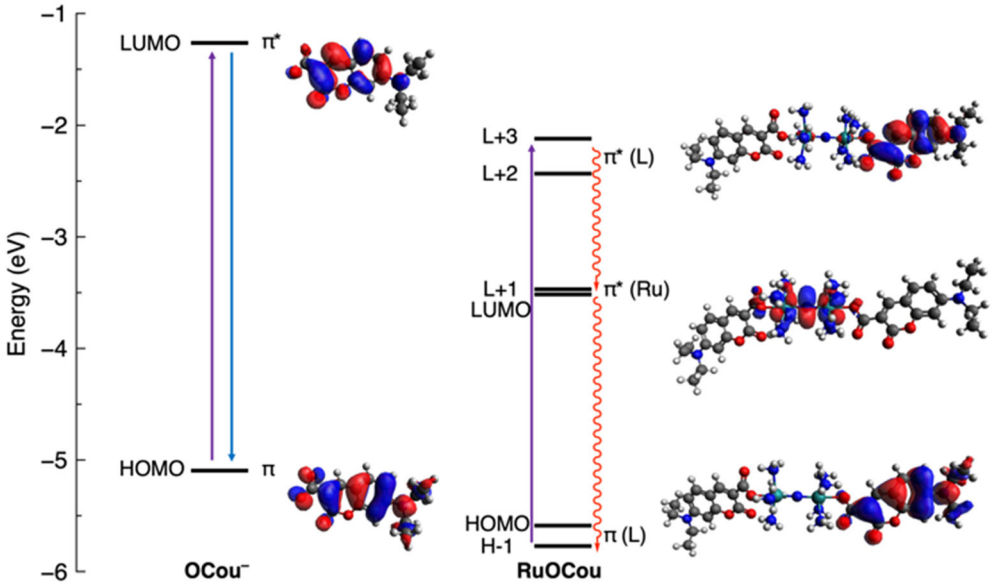

Figure 3.

Frontier Kohn-Sham molecular orbital diagrams of the coumarin-carboxylate ligand ($OCou^-$) and **RuOCou** with an isovalue of 0.02. Purple arrows: photoexcitation from ground state to the coumarin-based excited state. Blue arrow: electronic transition involved in fluorescence from the coumarin-based excited state. Red wavy arrows: electronic transitions involved in photoinduced electron transfer leading to non-radiative relaxation to the ground state.

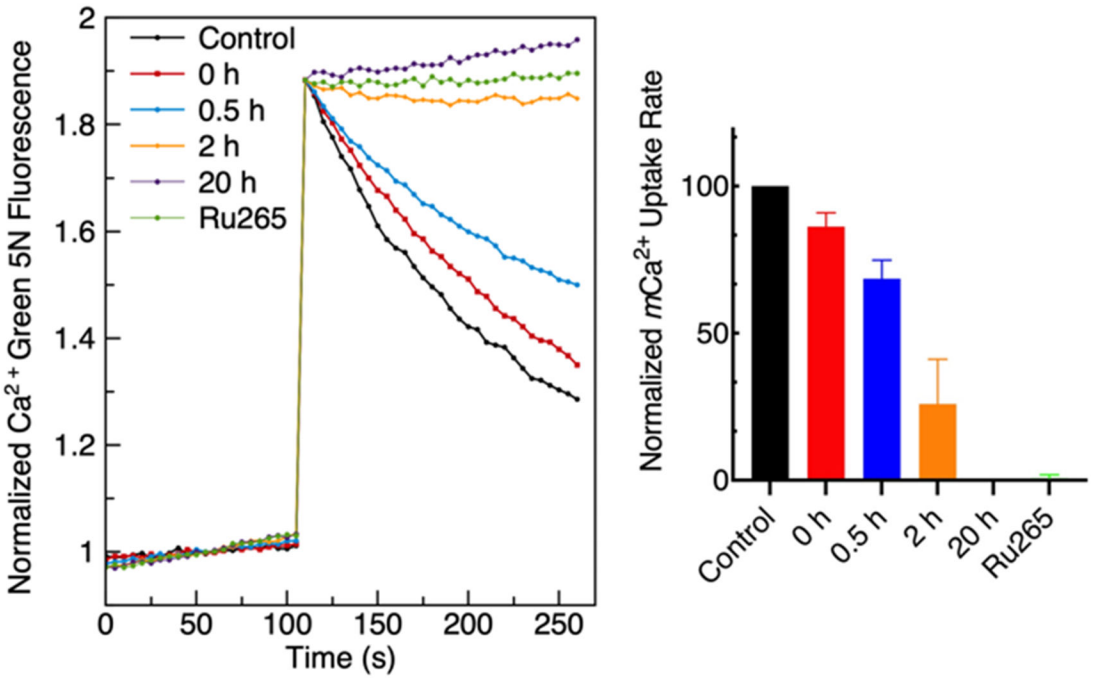

Figure 4.

Left: representative traces of extramitochondrial Ca^{2+} clearance after addition of 10 μM Ca^{2+} in permeabilized HEK293T cells treated with either 4 nM Ru265 or **RuOCou** prepared from stocks that had been pre-incubated at 37 °C (pH 7.4) for different durations. Right: *m*Ca^{2+} uptake rate based on the kinetics of extramitochondrial Ca^{2+} clearance. The *m*Ca^{2+} uptake rate of the untreated cells was normalized to 100.

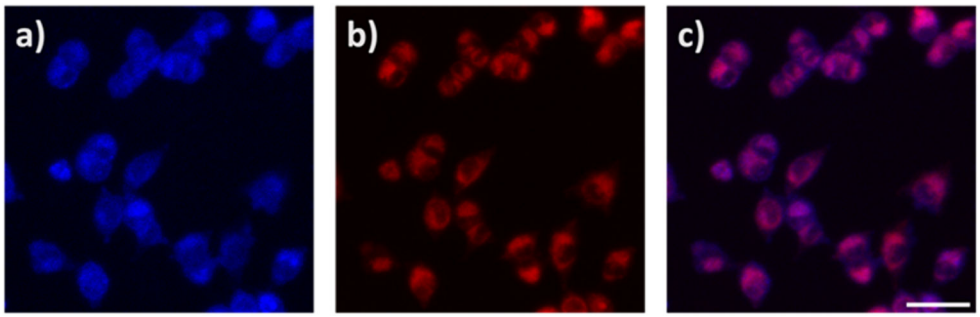

Figure 5.

Confocal fluorescent microscopy images of HeLa cells treated with 20 μM **RuOCou** (a) for 24 h and then MitoTracker Red (b) for 30 min. (c) is the overlaid image. Scale bar = 50 μm.

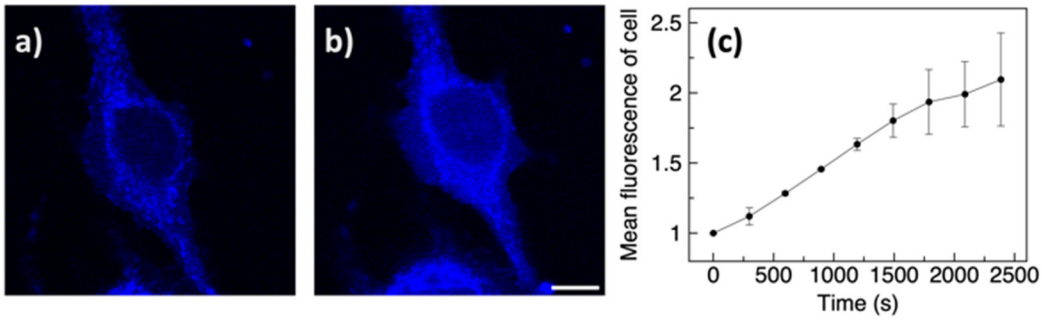

Figure 6.

Confocal fluorescent microscopy images of HeLa cells treated with 75 μM **RuOCou** for 30 min and subsequently imaged for 40 min. (a): image at 0 min. (b): image at 40 min. (c): mean fluorescence intensity versus time with the initial intensity normalized to 1. Scale bar = 10 μm.

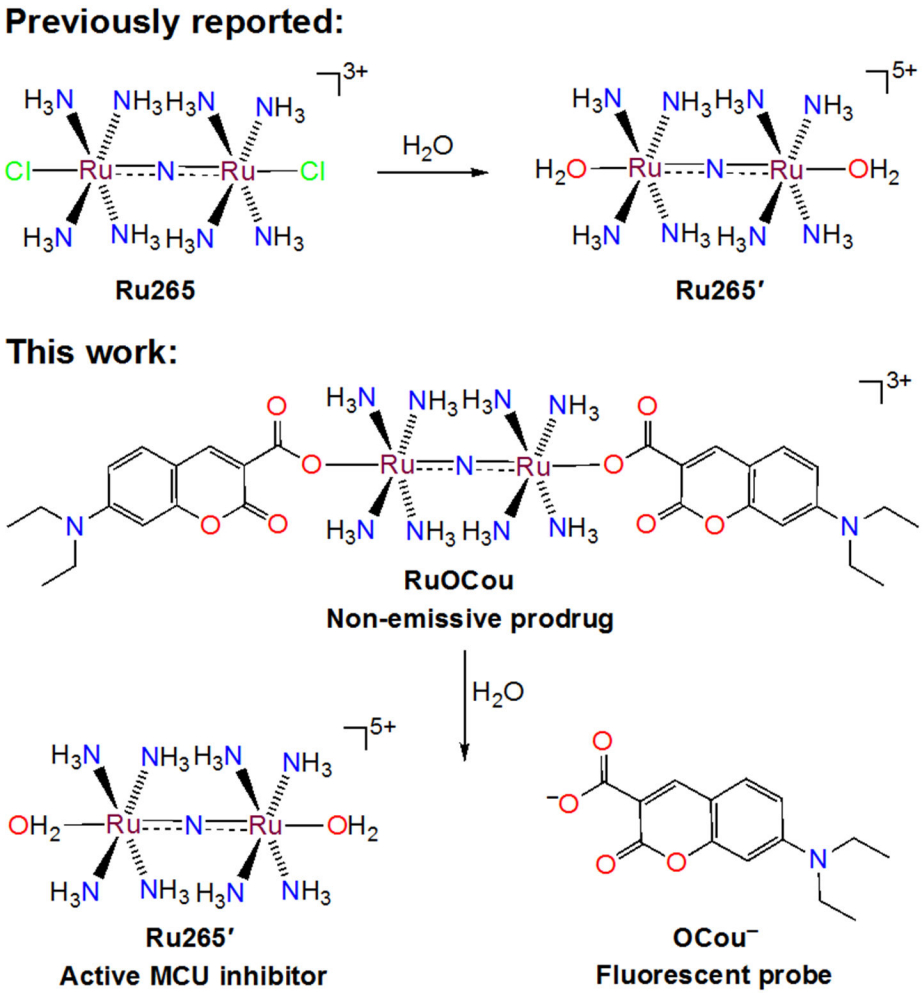

Scheme 1.
Activation pathways of Ru265 and **RuOCou**.

Table 1.

Relevant biological properties of Ru265 and **RuOCou**.

Property	Ru265	RuOCou
Aquation half-life[a]	2.3 min[b]	2.1 ± 0.05 h
mCa^{2+} inhibition IC_{50} (nM)[c]	2.2 ± 0.6	16.1 ± 3.6
Cytotoxicity IC_{50} (μM)[d]	195 ± 8[e]	55.5 ± 11.9
Cellular uptake (pg Ru / μg protein)	33 ± 7	395 ± 75

[a] pH 7.4 at 37°C.

[b] Ref[22].

[c] In permeabilized HEK293T cells, measured immediately after addition of the compound.

[d] In intact HEK293T cells after a 48 h incubation period.

[e] Ref[20].